ARMY RESEARCH LABORATORY

Phase-Field Analysis of Fracture-Induced Twinning in Single Crystals

by J. D. Clayton and J. Knap

ARL-RP-448 **July 2013**

A reprint from *Acta Materialia*, Vol. 61, pp. 5341–5353, 2013.

NOTICES

Disclaimers

The findings in this report are not to be construed as an official Department of the Army position unless so designated by other authorized documents.

Citation of manufacturer's or trade names does not constitute an official endorsement or approval of the use thereof.

Destroy this report when it is no longer needed. Do not return it to the originator.

Army Research Laboratory
Aberdeen Proving Ground, MD 21005-5069

ARL-RP-448 **July 2013**

Phase-Field Analysis of Fracture-Induced Twinning in Single Crystals

J. D. Clayton
Weapons and Materials Research Directorate, ARL

J. Knap
Computational and Information Sciences Directorate, ARL

A reprint from *Acta Materialia*, Vol. 61, pp. 5341–5353, 2013.

REPORT DOCUMENTATION PAGE

Form Approved
OMB No. 0704-0188

1. REPORT DATE *(DD-MM-YYYY)*	2. REPORT TYPE	3. DATES COVERED (From - To)
July 2013	Reprint	October 2012–May 2013

4. TITLE AND SUBTITLE
Phase-Field Analysis of Fracture-Induced Twinning in Single Crystals

5a. CONTRACT NUMBER

5b. GRANT NUMBER

5c. PROGRAM ELEMENT NUMBER

6. AUTHOR(S)
J. D. Clayton and J. Knap

5d. PROJECT NUMBER
AH80

5e. TASK NUMBER

5f. WORK UNIT NUMBER

7. PERFORMING ORGANIZATION NAME(S) AND ADDRESS(ES)
U.S. Army Research Laboratory
ATTN: RDRL-WMP-C
Aberdeen Proving Ground, MD 21005-5069

8. PERFORMING ORGANIZATION REPORT NUMBER
ARL-RP-448

9. SPONSORING/MONITORING AGENCY NAME(S) AND ADDRESS(ES)

10. SPONSOR/MONITOR'S ACRONYM(S)

11. SPONSOR/MONITOR'S REPORT NUMBER(S)

12. DISTRIBUTION/AVAILABILITY STATEMENT
Approved for public release; distribution is unlimited.

13. SUPPLEMENTARY NOTES
A reprint from *Acta Materialia*, Vol. 61, pp. 5341–5353, 2013.

14. ABSTRACT

Deformation twinning at the tip of a straight crack or notch is analyzed using a phase-field method that seeks equilibrium twin morphologies via direct minimization of a free energy functional. For isotropic solids, the tendency to twin under mode I or mode II loading is found to depend weakly on Poisson's ratio and elastic nonlinearity and strongly on surface energy and twinning shear (i.e., eigenstrain). Depending on the coherent twin boundary energy, anisotropy of surface energy is important for mode I loading but less so for mode II. Model predictions for several single crystals are in agreement with experimental observations. Calcite demonstrates a preference for mode I cleavage crack extension over crack tip twinning. Magnesium shows a likelihood for tensile twinning from a pre-existing crack on the basal plane. In sapphire, a preference for rhombohedral twins over basal twins is apparent, with the latter thinner in shape than the former.

15. SUBJECT TERMS
mesoscale modeling, fracture, twinning, ceramics, metals, phase field, crystals modeling, simulation

16. SECURITY CLASSIFICATION OF:			17. LIMITATION OF ABSTRACT	18. NUMBER OF PAGES	19a. NAME OF RESPONSIBLE PERSON
a. REPORT	b. ABSTRACT	c. THIS PAGE			J. D. Clayton
Unclassified	Unclassified	Unclassified	UU	18	19b. TELEPHONE NUMBER (*Include area code*) 410-278-6146

Available online at www.sciencedirect.com

SciVerse ScienceDirect

Acta Materialia 61 (2013) 5341–5353

Acta MATERIALIA

www.elsevier.com/locate/actamat

Phase-field analysis of fracture-induced twinning in single crystals

J.D. Clayton [a,*], J. Knap [b]

[a] Impact Physics, RDRL-WMP-C, US Army Research Laboratory, Aberdeen Proving Ground, MD 21005-5066, USA
[b] Computational Science and Engineering, RDRL-CIH-C, US Army Research Laboratory, Aberdeen Proving Ground, MD 21005-5066, USA

Received 22 March 2013; received in revised form 17 May 2013; accepted 18 May 2013
Available online 18 June 2013

Abstract

Deformation twinning at the tip of a straight crack or notch is analyzed using a phase-field method that seeks equilibrium twin morphologies via direct minimization of a free energy functional. For isotropic solids, the tendency to twin under mode I or mode II loading is found to depend weakly on Poisson's ratio and elastic nonlinearity and strongly on surface energy and twinning shear (i.e. eigenstrain). Depending on the coherent twin boundary energy, anisotropy of surface energy is important for mode I loading but less so for mode II. Model predictions for several single crystals are in agreement with experimental observations. Calcite demonstrates a preference for mode I cleavage crack extension over crack tip twinning. Magnesium shows a likelihood for tensile twinning from a pre-existing crack on the basal plane. In sapphire, a preference for rhombohedral twins over basal twins is apparent, with the latter thinner in shape than the former.
Published by Elsevier Ltd. on behalf of Acta Materialia Inc.

Keywords: Phase field; Twinning; Fracture; Crystals; Modeling and simulation

1. Introduction

Deformation twinning, i.e. twinning induced by mechanical stress, and cleavage fracture, i.e. transgranular fracture on preferred crystallographic planes, are two fundamental inelastic deformation mechanisms that may occur in crystals. In some cases, twins or twin boundaries may act as nucleation sites for fracture [1]; in others, crack tips may provide the necessary stress concentrations for twin nucleation and growth [2].

In dynamic experiments such as plate impact, both twinning and cleavage fracture may occur, but whether twinning precedes or follows fracture cannot usually be determined from analysis of experimental (e.g. Hugoniot) data and post-mortem material characterization. This is the case for impact experiments on sapphire [3], wherein theoretical strengths for twinning, slip and shear fracture are thought to be of the same order of magnitude [4]. Indentation experiments on ceramics and minerals often show evidence of both fracture and twinning, with surface damage strongly promoting the nucleation and growth of twins in calcite, for example [5,6].

The present work seeks (i) to develop an improved understanding of the general factors affecting twinning induced by fracture; and (ii) to test a predictive model for twinning at a crack/notch tip in several real materials. Phase-field theory and numerical simulation are applied to study twin nucleation and growth from a pre-existing crack or notch. A prior analysis [2] based on the Peierls–Nabarro concept and ideas from Ref. [7] was developed to judge the tendency of a solid to undergo either microtwinning or slip of leading and trailing partial dislocations on the same plane. This treatment demonstrated success for several face-centered cubic metals when compared to results of atomic simulations, but the model requires knowledge of parameters associated with the stacking fault energy surface that seem only to be obtainable from atomic simulation of planar defects. An analytical model

* Corresponding author. Tel.: +1 4102786146.
E-mail addresses: john.d.clayton1.civ@mail.mil (J.D. Clayton), jaroslaw.knap.civ@mail.mil (J. Knap).

1359-6454/$36.00 Published by Elsevier Ltd. on behalf of Acta Materialia Inc.
http://dx.doi.org/10.1016/j.actamat.2013.05.023

predicting the likelihood of twinning or extension of a mode I slit crack is described in Ref. [8]; this model requires knowledge of energetic data associated with total resistance to twinning or fracture that are evidently not available from standard experiments, though twin boundary and cleavage surface energies can be substituted as an approximation. As will be shown later, the current work offers more insight into the total twinning resistance that could be used in such a model.

In the present phase-field approach [9,10], the only constitutive model parameters are the twinning shear (usually known from crystallography), elastic constants (known from experiments), gradient energy coefficient(s), and double-well energy barrier height. The latter two can be related to the twin boundary surface energy (measurable from experiment or atomic simulation) and the thickness of the diffuse interface, which can be assigned physical significance if the normal distance from the phase/twin boundary over which atoms are displaced from their usual positions in a perfect crystal is known, e.g. from atomic simulation. For prescribed boundary conditions and problem geometry, the tendency for a pre-cracked crystal to continue to crack or to twin then necessarily depends on these parameters and the surface energy associated with cleavage fracture. The model does not depend on the numerical method of solution or grid size (i.e. the theory itself is mesh independent), but any discretization should be sufficiently refined to resolve continuum fields where gradients exist, e.g. in interfacial regions.

The present work does not address plastic slip distinct from the motion of twinning partials inherent in deformation twinning. Nanoscale treatments of discrete slip criteria include Refs. [2,7]; mesoscale continuum crystal plasticity models of slip and twinning are described in Ref. [11] and references therein.

Several other relevant modeling approaches are noted. Phase transformation has been studied at tips of moving cracks via analytical solutions to phase-field models [12,13]. Like twinning, phase transformations may be induced by strong local elastic fields at crack tips; transformation strain in the former often includes dilatation, while deformation twinning involves large shear without inelastic volume change. Competition among phase transformation, fracture and plastic deformation was studied using a continuum thermodynamic approach implemented in the finite-element method [14]; twinning was also modeled. Phase-field models of fracture have also been implemented [15–19]. The present paper does not develop a phase-field model for fracture—herein a stationary pre-crack is represented explicitly by a thin notch with free surface boundary conditions—but conceivably both twinning and fracture could be modeled simultaneously using the phase-field approach, with distinct order parameters accounting for transformation to twinned and/or fractured material.

This paper is organized as follows. The phase-field theory developed and implemented in Refs. [9,10] is reviewed in Section 2, including various elasticity models (linear isotropic, linear anisotropic, nonlinear neo-Hookean) considered later. Analysis of possible twinning or crack extension under pure mode I or mode II loading in generic isotropic elastic solids follows in Section 3. In this analysis, a normalized energy functional is derived that depends on several dimensionless material parameters. The effects of these parameters—twinning shear, Poisson's ratio and normalized twin boundary energy—on twinnability are investigated through phase-field simulations. In Section 4, two-dimensional (2-D) simulations of twinning from a mode I crack are reported for calcite ($CaCO_3$), sapphire (α-Al_2O_3) and magnesium (Mg) and compared with experimental observations. In Section 5, three-dimensional (3-D) simulations of basal and rhombohedral twinning in a sapphire single crystal with a pre-existing halfpenny-shaped notch are analyzed. Conclusions follow in Section 6. Regarding notation, vectors and second-order tensors are written in bold italic; scalars and components are written in plain italic, with summation applied over repeated indicial subscripts.

2. Theory

Only essential details of the phase-field theory are reported here; complete descriptions are given elsewhere [9,10]. Let $\boldsymbol{x}$ and $\boldsymbol{X}$ denote sufficiently smooth spatial and material coordinates of a body of reference volume Ω, related by the differentiable mapping $\boldsymbol{x} = \boldsymbol{\chi}(\boldsymbol{X}, t)$ that is one-to-one and invertible at any fixed t. Let $\eta(\boldsymbol{X}, t)$ denote the order parameter that distinguishes between the original (parent) crystal, the twin, and the interfacial boundary regions between parent and twin:

$$\eta = 0 \forall \boldsymbol{X} \in \text{ parent}, \qquad \eta = 1 \forall \boldsymbol{X} \in \text{ twin},$$
$$0 < \eta < 1 \forall \boldsymbol{X} \in \text{ boundary}. \tag{2.1}$$

The deformation gradient is

$$\boldsymbol{F} = \nabla \boldsymbol{\chi} = \boldsymbol{F}^E \boldsymbol{F}^\eta, \tag{2.2}$$

where ∇ denotes the material gradient, $\boldsymbol{F}^E$ accounts for elastic stretch and rotation, and

$$\boldsymbol{F}^\eta = \mathbf{1} + [\varphi(\eta)\gamma_0]\boldsymbol{s} \otimes \boldsymbol{m} \tag{2.3}$$

accounts for twinning shear. Orthogonal unit vectors (in material coordinates) in the twinning direction and normal to twinning plane are $\boldsymbol{s}$ and $\boldsymbol{m}$, the magnitude of maximum twinning shear is γ_0, and $\varphi(\eta)$ is an interpolator satisfying $\varphi(0) = 0$, $\varphi(1) = 1$, $\varphi'(0) = \varphi'(1) = 0$, where $(\cdot)' = \mathrm{d}(\cdot)/\mathrm{d}\eta$. Defining $\boldsymbol{C}^E = (\boldsymbol{F}^E)^{\mathrm{T}}\boldsymbol{F}^E$, the local ratio of deformed to initial volume is $J = \det \boldsymbol{F} = (\det \boldsymbol{C}^E)^{1/2}$.

The total energy functional for the body is

$$\Psi(\boldsymbol{\chi}, \eta) = \int_\Omega [W(\boldsymbol{F}, \eta) + f(\eta, \nabla\eta)]\mathrm{d}\Omega. \tag{2.4}$$

The strain energy W and interfacial energy f per unit reference volume are of the form

$$W = W[\boldsymbol{C}^E(\boldsymbol{F},\eta),\eta], \qquad f = f_0(\eta) + \boldsymbol{\kappa} : (\nabla\eta \otimes \nabla\eta). \tag{2.5}$$

Let $\partial\Omega$ denote the boundary of Ω. Imposing the variational principle

$$\delta\Psi = \oint_{\partial\Omega} (\boldsymbol{t}\cdot\delta\boldsymbol{\chi} + h\delta\eta)\mathrm{d}S, \tag{2.6}$$

the following local equilibrium equations and boundary conditions are derived [9]:

$$\nabla\cdot\partial W/\partial\boldsymbol{F} = \nabla\cdot\boldsymbol{P} = 0,$$
$$f_0' - 2\nabla\cdot(\boldsymbol{\kappa}\nabla\eta) + \partial W/\partial\eta = 0; \tag{2.7}$$
$$\boldsymbol{t} = \boldsymbol{P}\cdot\boldsymbol{n}, \qquad h = 2\boldsymbol{\kappa} : (\nabla\eta\otimes\boldsymbol{n}). \tag{2.8}$$

Traction per unit reference area is $\boldsymbol{t}$; conjugate force to the order parameter is h; outward normal to $\partial\Omega$ is $\boldsymbol{n}$. Phase equilibrium in (2.7) can be written for homogeneous $\boldsymbol{\kappa}$ as

$$f_0' = 2\boldsymbol{\kappa} : \nabla\nabla\eta + \tau\gamma_0\varphi',$$
$$\tau = \boldsymbol{S} : [\boldsymbol{C}^E(\boldsymbol{s}\otimes\boldsymbol{m})\boldsymbol{F}^{\eta\ -1}], \quad \boldsymbol{S} = 2\partial W/\partial\boldsymbol{C}^E. \tag{2.9}$$

In the present work, attention is restricted to a double-well potential $f_0 = A\eta^2(1-\eta)^2$, with A a constant related to the barrier height. When isotropic surface energy is imposed, for which $\boldsymbol{\kappa} = \kappa\boldsymbol{1}$, with κ a constant, then

$$f = A\eta^2(1-\eta)^2 + \kappa|\nabla\eta|^2, \qquad \kappa = 3\Gamma l/4,$$
$$A = 12\Gamma/l, \tag{2.10}$$

where Γ and l are equilibrium energy per unit area and thickness of an unstressed interface [9]. Anisotropic representations of surface energy are also considered. For example, in a material coordinate frame $\{\boldsymbol{e}_I\}$ with $\boldsymbol{e}_1\|\boldsymbol{s}$ and $\boldsymbol{e}_2\|\boldsymbol{m}$, then $\kappa_{11} > \kappa_{22}$ accounts for the increase in energy at an incoherent twin boundary [20] due to the local (e.g. core) energy of twinning dislocations [21], and $\kappa_{12} = \kappa_{21} = 0$ in this coordinate system.

Several different elastic models are considered [10]. For compressible neo-Hookean behavior

$$W = \frac{1}{2}\lambda[(\ln J)^2 + \mathrm{tr}\boldsymbol{C}^E - 3] - \mu\ln J, \tag{2.11}$$

where λ and μ are usual isotropic elastic constants. The First Piola–Kirchhoff stress is

$$\boldsymbol{P} = \partial W/\partial\boldsymbol{F} = \boldsymbol{F}^E\boldsymbol{S}\boldsymbol{F}^{\eta-\mathrm{T}}$$
$$= \boldsymbol{F}^E[\mu\boldsymbol{1} + (\lambda\ln J - \mu)\boldsymbol{C}^{E-1}]\boldsymbol{F}^{\eta-\mathrm{T}}. \tag{2.12}$$

For linear elastic behavior,

$$W = W[\boldsymbol{\epsilon}^E(\nabla\boldsymbol{u},\eta),\eta] = \frac{1}{2}\mathsf{C}_{IJKL}(\eta)\epsilon^E_{IJ}\epsilon^E_{KL}, \tag{2.13}$$

where the following geometric relationships apply:

$$\boldsymbol{F} = \boldsymbol{1} + \nabla\boldsymbol{u} \simeq \boldsymbol{1} + \boldsymbol{\beta}^E + \boldsymbol{\beta}^\eta; \tag{2.14}$$
$$\boldsymbol{F}^E \simeq \boldsymbol{1} + \boldsymbol{\beta}^E, \quad \boldsymbol{\epsilon}^E = \frac{1}{2}[\boldsymbol{\beta}^E + (\boldsymbol{\beta}^E)^{\mathrm{T}}], \quad \boldsymbol{C}^E \simeq \boldsymbol{1} + 2\boldsymbol{\epsilon}^E; \quad \boldsymbol{F}^\eta = \boldsymbol{1} + \boldsymbol{\beta}^\eta; \tag{2.15}$$
$$\boldsymbol{P} = \partial W/\partial\nabla\boldsymbol{u}, \quad \tau = \boldsymbol{P} : (\boldsymbol{s}\otimes\boldsymbol{m}). \tag{2.16}$$

For anisotropic elasticity, second-order coefficents C_{IJKL} are interpolated between parent and twinned domains using φ [9,10]. For isotropic elasticity, $\mathsf{C}_{IJKL} = \lambda\delta_{IJ}\delta_{KL} + \mu(\delta_{IK}\delta_{JL} + \delta_{IL}\delta_{JK})$, and W and C_{IJKL} do not depend explicitly on η. The elastic driving force for twinning, τ, is the resolved shear stress on the twinning plane in the direction of twinning shear.

Two different interpolation functions are also considered:

$$\varphi = (3-2\eta)\eta^2 \qquad \text{(polynomial)}, \tag{2.17}$$
$$\varphi = 1/[1 + \mathrm{e}^{-2k(\eta-0.5)}] \qquad \text{(exponential)}. \tag{2.18}$$

Polynomial function (2.17) has been used frequently [9,10,22] and yields a gradual change in φ over $0 < \eta < 1$; the Fermi–Dirac function (2.18), here with $k = 15$, provides a steeper increase in φ at $\eta \approx 0.5$, as is clear from Fig. 1.

Solutions to governing equations are obtained numerically using the finite-element method. The solution procedure [9] involves minimization of free energy functional Ψ, subject to possible boundary conditions/constraints, over domain Ω, yielding the equilibrium fields $(\boldsymbol{\chi}, \eta)$. Kinetics and dissipation are not quantified explicitly.

3. Twinning under mode I and II loading in isotropic solids

3.1. Dimensionless parameters

Consider the phase-field theory of Section 2 applied to an isotropic solid. Dividing by the shear modulus, a normalized free energy functional becomes

$$\bar{\Psi} = \Psi/\mu = \int_\Omega (\overline{W} + \bar{f})\mathrm{d}\Omega, \tag{3.1}$$
$$\overline{W} = \frac{\nu}{1-2\nu}(\mathrm{tr}\nabla\boldsymbol{u})^2 + (\nabla\boldsymbol{u} - \gamma_0\varphi\boldsymbol{s}\otimes\boldsymbol{m})_{\mathrm{s}} : (\nabla\boldsymbol{u} - \gamma_0\varphi\boldsymbol{s}\otimes\boldsymbol{m})_{\mathrm{s}}, \tag{3.2}$$
$$\bar{f} = \overline{A}\eta^2(1-\eta)^2 + \bar{\kappa}l^2|\nabla\eta|^2, \tag{3.3}$$
$$\nu = \lambda/(2\lambda+2\mu), \quad \overline{A} = A/\mu = 12\Gamma/(\mu l), \quad \bar{\kappa} = \kappa/(\mu l^2) = 3\Gamma/(4\mu l). \tag{3.4}$$

Notation $(\cdot)_{\mathrm{s}}$ denotes the symmetric part of a second-order tensor. Since $\mu > 0$, a solution $(\boldsymbol{u}, \eta)$ for a given set of boundary conditions on $\partial\Omega$ that minimizes Ψ also minimizes $\bar{\Psi}$; this could be a local (metastable) or global (stable) minimum energy configuration.

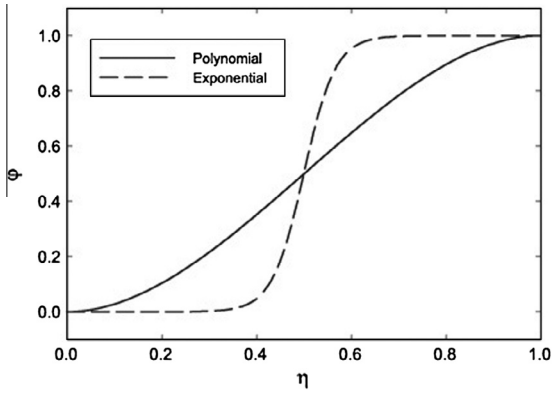

Fig. 1. Phase-field interfacial interopolation functions (2.17) and (2.18).

Let Γ_0 denote a constant reference value of twin boundary surface energy per unit area, and let $\overline{A}_0$ and $\bar{\kappa}_0$ denote the corresponding values of parameters in (3.4) for fixed $\mu = \mu_0$ and fixed l. Then

$$\Gamma/\Gamma_0 = \overline{A}/\overline{A}_0 = \bar{\kappa}/\bar{\kappa}_0. \tag{3.5}$$

In all subsequent analysis l is held fixed. In what follows, representative values of $\Gamma_0 = 100\ \mathrm{mJ\ m^{-2}}$ and $\mu_0 = 25$ GPa, with $l = 1.0$ nm [9,10,22], are used to establish $\overline{A}_0$ and $\bar{\kappa}_0$. During simulations, the effect of surface energy is then studied by varying Γ/Γ_0. In most simulations, isotropic surface energy is assumed, but in some (2-D) simulations, $\kappa_{11} = \alpha\kappa_{22} = \alpha\kappa$ is prescribed, where $\alpha > 1$ accounts for incoherent boundary energy as noted in Section 2. (For a twin system oriented differently from $\boldsymbol{s}\|\boldsymbol{e}_1$ and $\boldsymbol{m}\|\boldsymbol{e}_2$, $\boldsymbol{\kappa}$ is rotated as a second-order tensor.) Accordingly, for a given set of boundary conditions and prescribed initial crystal orientation ($\boldsymbol{s}$, $\boldsymbol{m}$), solutions thus obtained depend on the parameter set (γ_0, ν, Γ/Γ_0, α) and choice of interpolation function φ. The same arguments apply for the isotropic neo-Hookean elastic model of Section 2.

Plane-strain simulations of an initially square domain Ω of size $2a \times 2a$ are reported in Section 4. The domain contains a pre-existing straight edge crack of length a and thickness $2r_0$, with a rounded tip of radius r_0. The crack is assigned a finite radius for two reasons: (i) a perfect slit crack would result in truly singular stress fields at the tip that cannot be fully resolved with conventional finite elements; and (ii) in a real material a finite r_0 on the order of or exceeding a lattice parameter is expected since the separation distance across opposite faces of the crack should exceed a cut-off distance for interatomic cohesive forces that would otherwise result in traction across opposing faces of the crack.

Let the origin of reference coordinate systems ((r, θ) in polar form or (X, Y) in rectangular form) be located at the crack tip. Boundary conditions are imposed as follows. The crack surface Ξ ($\theta = \pm\pi$ rad, $0 < r < a$) is free of traction ($\boldsymbol{t} = \boldsymbol{0}$). Neumann conditions $h = 0$ for conjugate force to the order parameter are assigned along all of $\partial\Omega$. Along external boundary $\partial\Omega\backslash\Xi$ corresponding to X, $Y = \pm a$, displacements $\hat{\boldsymbol{u}}(r, \theta)$ corresponding to the K field for pure mode I or mode II loading [23] are imposed. For mode I:

$$\hat{u}_X = 2\Delta[ar/(2\pi)]^{1/2}\cos(\theta/2)[1 - 2\nu + \sin^2(\theta/2)], \tag{3.6}$$

$$\hat{u}_Y = 2\Delta[ar/(2\pi)]^{1/2}\sin(\theta/2)[2 - 2\nu - \cos^2(\theta/2)], \tag{3.7}$$

$$\Delta = K_{\mathrm{I}}/(2\mu a^{1/2}). \tag{3.8}$$

For mode II:

$$\hat{u}_X = 2\Delta[ar/(2\pi)]^{1/2}\sin(\theta/2)[2 - 2\nu + \cos^2(\theta/2)], \tag{3.9}$$

$$\hat{u}_Y = -2\Delta[ar/(2\pi)]^{1/2}\cos(\theta/2)[1 - 2\nu - \sin^2(\theta/2)], \tag{3.10}$$

$$\Delta = K_{\mathrm{II}}/(2\mu a^{1/2}). \tag{3.11}$$

For both modes, the orientation of the twin system ($\boldsymbol{s}$, $\boldsymbol{m}$) is such that the resolved shear stress τ of (2.16) is maximum according to the linear elastic solution [23]. For mode II, $\boldsymbol{s}$ is simply oriented in the sense of positive r along $\theta = 0$. For mode I, $\boldsymbol{s}$ is oriented in the sense of positive r along $\theta = 1.22$ rad.

During phase-field simulations, Δ is increased incrementally. For each increment, the domain is seeded with a small twin nucleus at $r \leqslant r_0$. Displacement boundary conditions are updated according to the mode of loading via (3.6), (3.7), (3.8) or (3.9), (3.10), (3.11), and then the equilibrium solution ($\boldsymbol{u}$, η) in Ω is obtained through energy minimization using the finite-element method. If the driving force for twinning is insufficient, then the initial nucleus will disappear, and the equilibrium solution includes $\eta = 0 \forall \boldsymbol{X} \in \Omega$. Otherwise, at a threshold load parameter $\Delta = \Delta_{\mathrm{T}}$, a stable twin will appear at the crack tip ($r = 0$). With further increasing $\Delta > \Delta_{\mathrm{T}}$, the twin will grow in length and/or thickness until it interacts with the external boundary $\partial\Omega\backslash\Xi$.

According to linear elastic fracture mechanics, crack extension (i.e. cleavage) will occur if the applied stress intensity factor or corresponding strain energy release rate exceeds a threshold for a particular material and loading mode:

$$K_{\mathrm{I/II}} \geqslant K_{\mathrm{C}} \Longleftrightarrow G_{\mathrm{I/II}} \geqslant G_{\mathrm{C}} \Rightarrow \text{fracture}, \tag{3.12}$$

where the fracture surface energies are

$$G_{\mathrm{I/II}} = K_{\mathrm{I/II}}^2(1 - \nu)/(2\mu),$$
$$G_{\mathrm{C}} = K_{\mathrm{C}}^2(1 - \nu)/(2\mu), \tag{3.13}$$

and here no distinction has been made in notation among threshold fracture energies G_{C} for different modes. For comparison, dimensionless twinning and fracture parameters associated with the normalized strain energy required for either mechanism can be constructed:

$$\overline{\Gamma}_{\mathrm{T}} = \Gamma_{\mathrm{T}}/(\mu l) = a(1 - \nu)\Delta_{\mathrm{T}}^2/l, \qquad \overline{G}_{\mathrm{C}} = G_{\mathrm{C}}/(\mu l). \tag{3.14}$$

The following criteria then emerge that predict either crack extension or twin emission from the crack tip:

$$2\overline{\Gamma}_{\mathrm{T}}/\overline{G}_{\mathrm{C}} = 2\Gamma_{\mathrm{T}}/G_{\mathrm{C}} \gg 1 \Rightarrow \text{fracture},$$
$$2\overline{\Gamma}_{\mathrm{T}}/\overline{G}_{\mathrm{C}} = 2\Gamma_{\mathrm{T}}/G_{\mathrm{C}} \ll 1 \Rightarrow \text{twinning}. \tag{3.15}$$

Dimensionless $\overline{\Gamma}_{\mathrm{T}}$ can be interpreted as an inverse measure of the "twinnability" of a given material subjected to mode I or mode II loading, with smaller values of $\overline{\Gamma}_{\mathrm{T}}$ denoting an increased tendency for crack tip twinning. The factor of two arises because, in the usual convention of fracture mechanics, the strain energy release rate G_{C} is twice the fracture surface energy Γ_{C}. (In this paper, notation "Γ" is associated generically with surface energy, "G" with strain energy release.) When $2\overline{\Gamma}_{\mathrm{T}} \approx \overline{G}_{\mathrm{C}}$, strain energy released by twinning and crack extension are comparable, and either mechanism could be expected to occur. Note that because $\Delta \propto a^{-1/2}$, imposed displacements $\hat{\boldsymbol{u}}$ and twinning resistance $\overline{\Gamma}_{\mathrm{T}}$ do not depend on a, which serves merely as a normalization constant to render these quantities dimensionless.

In phase-field simulations, meshes are used with significant refinement (element size $\ll l$) near the crack tip and along the anticipated path of twin extension, such that solutions are independent of mesh resolution. Twin nucleation depends strongly on local fields near $r = 0$ but not strongly on a; further increasing the domain size above $a/l = 50$ did not significantly affect initial stages of twinning, but as the twin grows and approaches the boundary, the choice of a necessarily affects the solution. Solutions can be modestly dependent on notch radius for small r_0, so two choices of r_0 are explored. Tables 1 and 2 list parameters investigated in simulations reported subsequently in Section 4. The typical (i.e. usual) parameter set referred to as "linear elastic" in subsequent figures is given in Table 1. Normalized twin boundary energy is $\overline{\Gamma}_0 = \Gamma/(\mu l)$. Deviations from these parameters referred to in some later figures are explained in Table 2. In particular, the value of $\alpha = 100$ follows from Refs. [20,21].

3.2. Numerical results

Figs. 2 and 3 show characteristic results for mode I and mode II loading, respectively. The undeformed finite-element (FE) mesh is shown in part (a) of each figure. Twin morphology and a stress component—tensile stress for mode I, shear stress for mode II—are shown in parts (b) and (c), corresponding to a load increment exceeding nucleation, i.e. $\Delta > \Delta_T$. In each case, the twin (i.e. stress-free shear eigenstrain $\gamma_0/2$) relieves much of the stress that would otherwise be large as $r \to 0$ in an elastic medium without a twin. Twin growth to the boundary $\partial\Omega$ is inhibited by the displacement boundary conditions.

Twin morphologies for various simulations of mode I deformation are compared at the same load increment $\Delta = 0.04 > \Delta_T$, i.e. at the same imposed K_I, in Fig. 4. Because differences in twin size and shape are small, it is concluded that model predictions of fully formed twin morphology are not sensitive to choice of linear or nonlinear (i.e. neo-Hookean) elastic model, choice of interpolation function (2.17) or (2.18), twin boundary surface energy anisotropy α, or pre-existing thickness of the crack or notch. However, as discussed later, twin nucleation is affected by these choices in some cases.

Fig. 5 shows the effects of dimensionless material properties on twinning resistance $2\overline{\Gamma}_T$ of (3.14) under mode I loading. Recall from (3.15) that this resistance can be compared with $\overline{G}_C$ to predict whether twinning or cleavage crack extension would be energetically favorable, with smaller $\overline{\Gamma}_T$ suggesting a greater tendency for twinning at the crack tip. Each data point on each piecewise linear curve in Fig. 5 represents the result of a different phase-field simulation in which Δ (i.e. K_I) is increased in increments of 10^{-3} from $\Delta = 0$ to the condition for which a twin or twin nucleus is first observed at $\Delta = \Delta_T$.

Table 1
Basic simulation parameters.

Descriptor	Elasticity model	φ	r_0/l	α	$\overline{\Gamma}_0$
Linear elastic	Linear isotropic	Polynomial	2	1	4×10^{-3}

Table 2
Other simulation parameters.

Descriptor	Difference from basic parameters
Neo-Hookean	Neo-Hookean elastic energy
Exponential interpolant	Exponential φ
Anisotropic $\boldsymbol{\kappa}$	$\alpha = \kappa_{11}/\kappa_{22} = 100$
Thin notch	$r_0/l = 0.5$

Effects of twinning shear γ_0 on crack tip twinnability are shown in Fig. 5a, where discrete values of $\gamma_0 = (0.1, 0.3, 0.5, 0.7, 1.0)$ have been prescribed in simulations incorporating linear elastic or neo-Hookean strain energy density W. Twinning shear significantly affects nucleation. A minimum of twinning resistance $\overline{\Gamma}_T$ is predicted at $\gamma_0 = 0.3$ for each model. For $\gamma_0 < 0.3$, resistance increases since the eigenstrain does not reduce elastic energy so much. Nucleation resistance also increases for $\gamma_0 > 0.3$, presumably because the applied K_I field must be sufficiently strong such that a large eigenstrain relieves the elastic stress field induced by the crack.

The effects of Poisson's ratio ν on twin nucleation resistance are comparatively small, as shown in Fig. 5b for values of $\nu = (0.05, 0.15, 0.25, 0.35, 0.45)$. The low influence of Poisson's ratio on twinning found here agrees with conclusions of a previous linear elastic analysis [24]. Neo-Hookean elasticity is more sensitive than linear elasticity to ν, as expected considering the nonlinear compressibility inherent in (2.11).

As shown in Fig. 5c, twin boundary energy Γ_0 strongly affects twinnability, with resistance $\overline{\Gamma}_T$ increasing with increasing Γ/Γ_0 in all cases. Discrete values $\Gamma/\Gamma_0 = (0.5, 0.75, 1, 1.5, 2)$ have been probed. Twinning resistance increases relative to the linear elastic case when the exponential interpolator of (2.18), anisotropic surface energy ($\alpha = 100$) or a thinner notch/crack is used. Differences increase as the ratio Γ/Γ_0 increases.

Fig. 6 shows effects of dimensionless material properties on twinning resistance $2\overline{\Gamma}_T$ of (3.14) under mode II loading, and is analogous to results for mode I of Fig. 5. Again, each data point represents the result of a different phase-field simulation in which Δ (here proportional to K_{II}) is increased in increments of 1×10^{-3} from $\Delta = 0$ to the condition for which a twin or twin nucleus is first observed at $\Delta = \Delta_T$.

The effects of twinning shear γ_0 on crack tip twinnability are shown in Fig. 6a, where discrete values of $\gamma_0 = (0.1, 0.3, 0.5, 0.7, 1.0)$ have been prescribed in simulations incorporating linear elastic or neo-Hookean strain energy W. Twinning shear significantly affects mode II nucleation, as was the case for mode I. Here, a minimum of twinning resistance $\overline{\Gamma}_T$ is predicted at $\gamma_0 = 0.5$ for each model in mode II loading, which exceeds the minimum associated $\gamma_0 = 0.3$ observed for mode I.

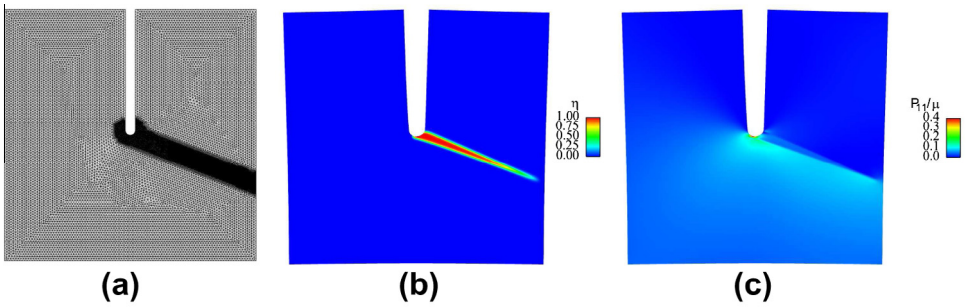

Fig. 2. Mode I loading of isotropic elastic solid $\left[\gamma_0 = \frac{1}{2}, \nu = \frac{1}{4}, \Gamma = \Gamma_0\right]$: (a) finite-element mesh; (b) order parameter at $\Delta = 0.05$; (c) tensile normal stress ($P_{11} = P_{YY}$) at $\Delta = 0.05$. The origin of the (X, Y) coordinate system is at the crack tip, with positive X downward and positive Y to the right. For polar (r, θ) coordinates, θ is measured counterclockwise from the positive X-axis.

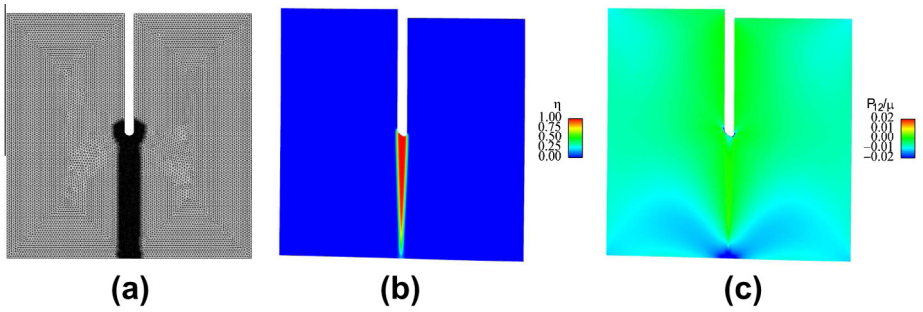

Fig. 3. Mode II loading of isotropic elastic solid $\left[\gamma_0 = \frac{1}{2}, \nu = \frac{1}{4}, \Gamma = \Gamma_0\right]$: (a) finite-element mesh; (b) order parameter at $\Delta = 0.03$; (c) shear stress ($P_{12} = P_{XY} = P_{YX}$) at $\Delta = 0.03$. The origin of the (X, Y) coordinate system is at the crack tip, with positive X downward and positive Y to the right. For polar (r, θ) coordinates, θ is measured counterclockwise from the positive X-axis.

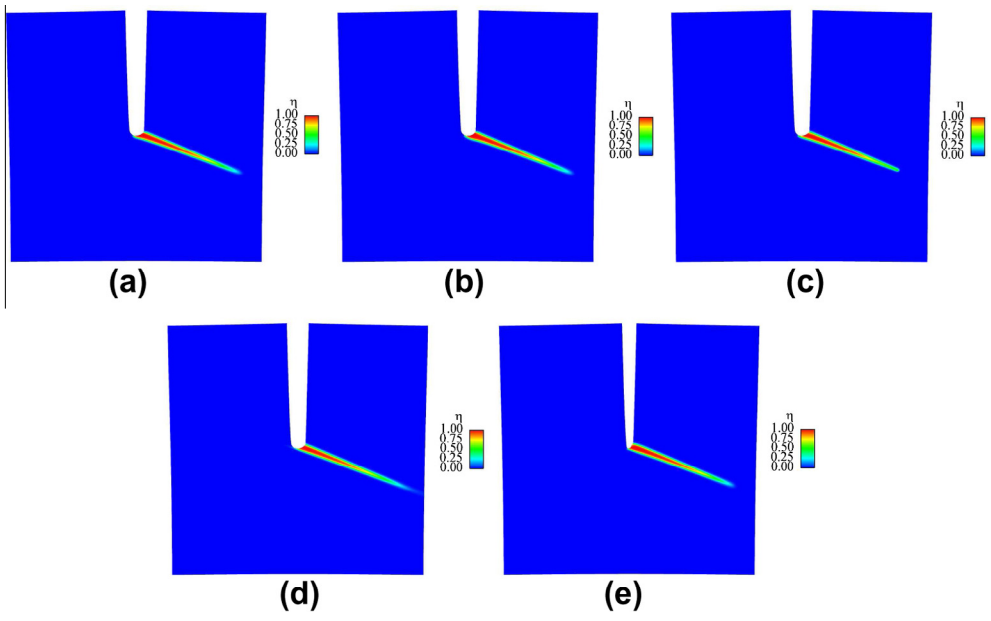

Fig. 4. Order parameter (twin morphology) for mode I loading of isotropic elastic solid at $\Delta = 0.04$ $\left[\gamma_0 = \frac{1}{2}, \nu = \frac{1}{4}, \Gamma = \Gamma_0\right]$: (a) linear elastic; (b) neo-Hookean; (c) exponential interpolant; (d) anisotropic κ; (e) thin notch.

The effects of Poisson's ratio ν on twin nucleation resistance under mode II loading are comparatively small, as shown in Fig. 6b. Twinning resistance for neo-Hookean elasticity is again more sensitive than linear elasticity to ν.

As shown in Fig. 6c, twin boundary energy Γ_0 strongly affects twinnability, with resistance $\overline{\Gamma}_T$ increasing with increasing Γ/Γ_0 in all cases, as was observed for mode I. Twinning resistance increases relative to the linear elastic

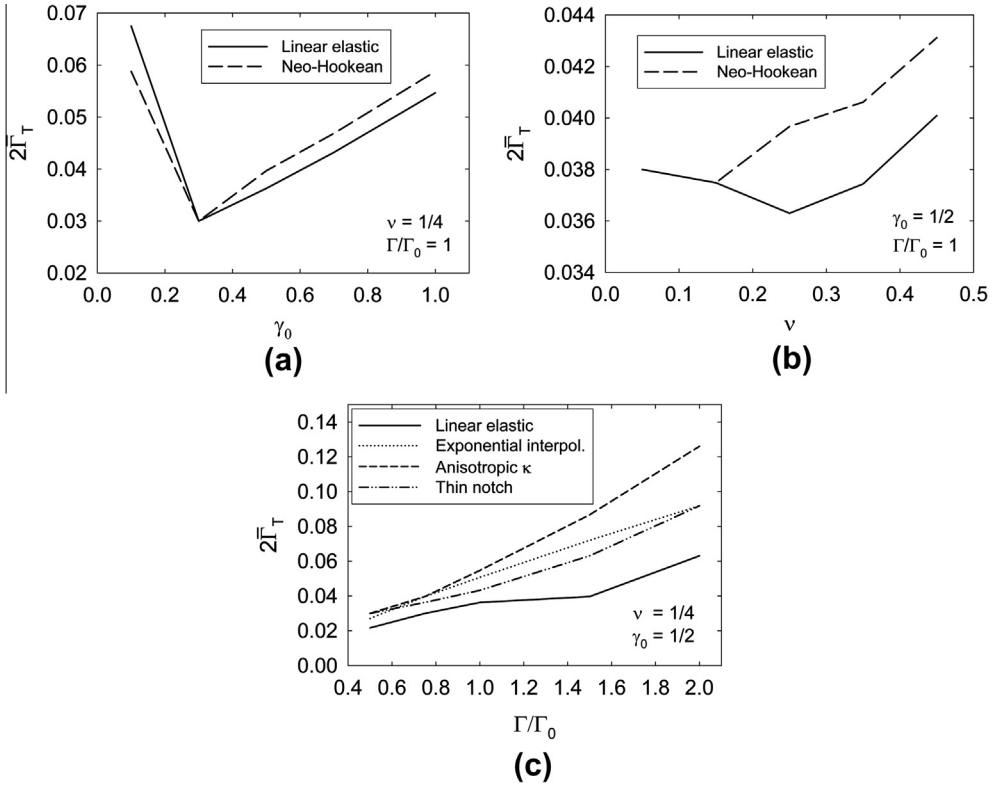

Fig. 5. Normalized twin nucleation energy $\overline{\Gamma}_T$ under mode I loading for (a) variable twinning shear γ_0; (b) variable Poisson's ratio ν; and (c) variable twin boundary surface energy Γ. A low value of $\overline{\Gamma}_T$ correlates with a low value of applied K_I needed to initiate a twin at the crack tip.

case when the exponential interpolator of (2.18) or anisotropic surface energy ($\alpha = 100$) is used, though the latter influences the results modestly and only for $\Gamma/\Gamma_0 > 1$. Contrary to results for mode I loading, a thinner notch reduces rather than increases twin resistance under mode II. Differences among cases in Fig. 6c increase as Γ/Γ_0 increases.

Comparing results in Figs. 5 and 6, numerical values of resistance to twinning $\overline{\Gamma}_T$ under mode I loading tend to exceed those under mode II by a factor of the order of 2. For example, for linear elasticity with the parameter set $[\gamma_0 = \frac{1}{2}, \nu = \frac{1}{4}, \Gamma = \Gamma_0]$, phase-field simulations predict $\overline{\Gamma}_T \approx 0.007$ for mode II and $\overline{\Gamma}_T \approx 0.011$ for mode I. This result is not unexpected since a minimum twinning resistance would be associated with the geometry of mode II loading in Fig. 3, i.e. with the twin system aligned perfectly with maximum shear stress at the tip of a mode II crack.

4. Twinning under mode I loading in single crystals

Twinning under mode I loading of a square domain with pre-existing edge crack is investigated next for single crystals with relevant physical properties. Plane-strain simulations on a sample of dimensions identical to that of Section 3 are reported. In this 2-D idealization, only one twin system is permitted to be active in any simulation, and the crack propagation direction in a particular cleavage plane is chosen such that crack opening is in the plane $\theta = \pm\pi$ rad, i.e. the pre-existing crack is along $Y = 0$, $X < 0$. Details regarding properties and results are reported in Table 3; corresponding discussion for each material follows next. As will become clear later, "Model" in Table 3 designates the type of elasticity model and/or twin boundary surface energy representation, with "isotropic" referring to isotropic linear elasticity and isotropic surface energy ($\alpha = 1$), "aniso. W" referring to anisotropic linear elasticity and isotropic surface energy, and "$\alpha = 100$" denoting isotropic linear elasticity with anisotropic surface energy.

4.1. Calcite

Calcite is a soft mineral of trigonal symmetry whose pure crystals are transparent. Calcite twins readily, with little or no plastic slip, under concentrated surface loading. The preferred twin system is e^+, with relatively large shear $\gamma_0 = 0.694$ and geometry $\langle 10\bar{1}0\rangle\{0001\}$ in rhombohedral pseudocell notation [25]. Calcite also cleaves easily on the natural rhombohedral planes (i.e. $\{10\bar{1}0\}$ planes) of its primitive unit cell, equivalent to $\{10\bar{1}1\}$ planes in the hexagonal notation of Refs. [26,27]. In the present simulations, a 2-D projection is required, where $\theta = 0.89$ rad is the resulting orientation of the e^+ twin system that receives the maximum stress τ under mode I loading of a cleavage plane. Cleavage surface energy entering $\overline{G}_C$ in Table 3 is obtained from experiments [27]. Properties associated with twinning and elasticity are from Ref. [10] and references

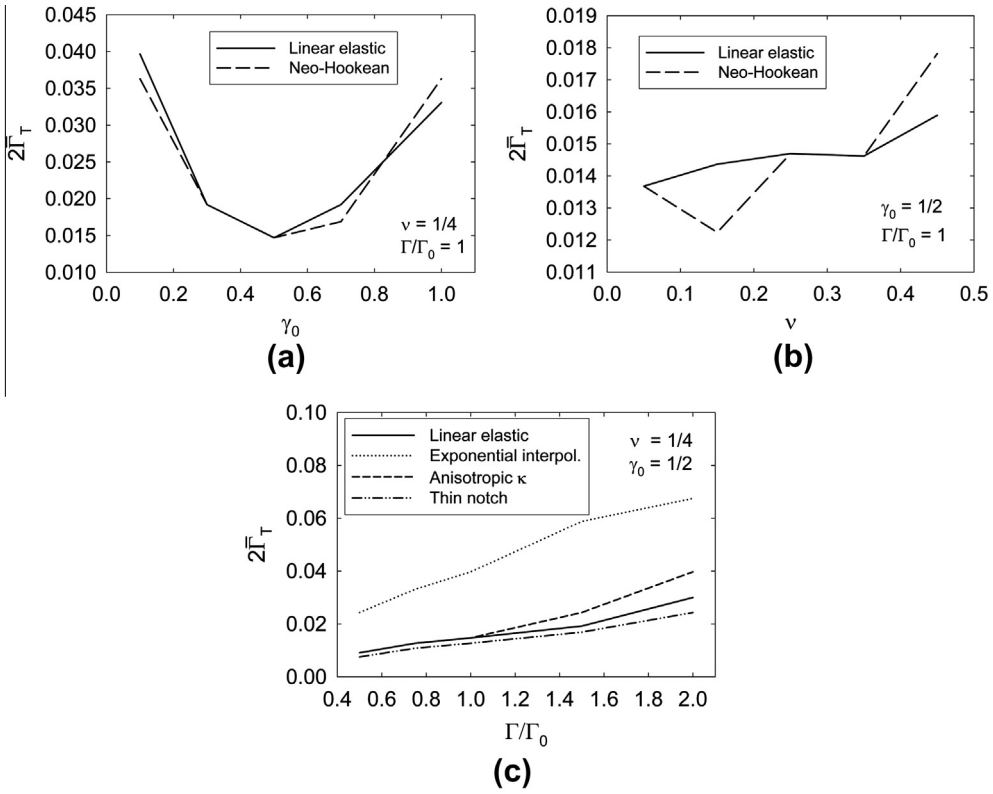

Fig. 6. Normalized twin nucleation energy $\overline{\Gamma}_T$ under mode II loading for (a) variable twinning shear γ_0; (b) variable Poisson's ratio ν; (c) variable twin boundary surface energy Γ. A low value of $\overline{\Gamma}_T$ correlates with a low value of applied K_{II} needed to initiate a twin at the crack tip.

Table 3
Single-crystal properties and results of phase-field simulations.

Material	ν	μ (GPa)	Crack	$\overline{G}_C$	Twin system	γ_0	$2\overline{\Gamma}_0$	Model	$2\overline{\Gamma}_T/\overline{G}_C$	Prediction
Calcite	0.30	40	$(10\bar{1}1)$	0.017	e^+	0.694	0.0091	aniso. W	2.53	Fracture
								Isotropic	2.96	Fracture
Sapphire	0.23	167	(0001)	0.48	Rhomb. (R)	0.202	0.0015	Isotropic	0.02	Twinning
			Max. τ	0.1				$\alpha = 100$	0.11	Twinning
			$(10\bar{1}2)$	0.072	Basal (B)	0.635	0.0089	Isotropic	0.62	Either
			Max. τ	0.1				$\alpha = 100$	0.65	Either
Mg	0.28	19	(0001)	382	$[10\bar{1}1](\bar{1}012)$	0.130	0.0121	Isotropic	2×10^{-4}	Twinning

therein. Both isotropic and anisotropic elastic models are investigated (i.e. forms of W). For the former, the Voigt elastic constants shown in Table 3 apply. For the latter, values ($C_{11} = 165$, $C_{12} = 65$, $C_{13} = 62$, $C_{14} = -23$, $C_{33} = 89$, $C_{44} = 37$ GPa) from Ref. [10] are used. For either elastic model, the displacement field of (3.6) and (3.7) is applied by incrementally increasing Δ or, equivalently, K_I; this is an approximation of the true K_I field when anisotropic elasticity is used.

Results in Fig. 7a and b show the twin at loading soon after nucleation, i.e. at $\Delta = 0.044 \gtrsim \Delta_T$. Nucleation occurs first for the anisotropic model, but the orientation ($\theta \approx 0.9$ rad) and shape of the twin are similar in each case. A secondary twin belonging to the same twin system begins to form at a larger applied K_I field, as shown in Fig. 7c. For anisotropic and isotropic models, $2.5 \lesssim 2\overline{\Gamma}_T/\overline{G}_C \lesssim 3$, meaning that crack extension is preferred over twinning according to criterion (3.15). This result is in qualitative agreement with tensile fracture experiments [26,27] that report no evidence of twinning. Parting fractures induced by twins in calcite have also been noted [28]. These model results do not contradict the possibility of twins induced by defects during other modes of loading, e.g. under spherical indentation, samples with visible surface cracks are known to twin more easily than those without [5].

4.2. Sapphire

Sapphire, also known as corundum or single-crystal alumina, is a hard ceramic/mineral that, like calcite, is of tri-

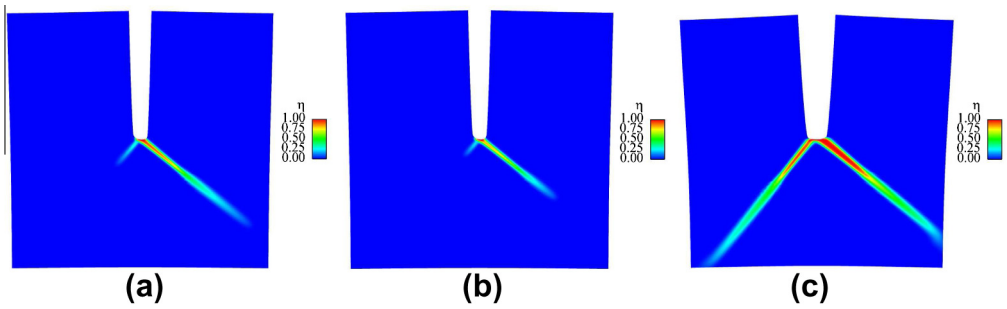

Fig. 7. Order parameter for mode I cleavage of calcite single crystal: (a) anisotropic elasticity, $\Delta = 0.044$; (b) isotropic elasticity, $\Delta = 0.044$; (c) isotropic elasticity, $\Delta = 0.1$.

gonal elastic symmetry and can be transparent. As reviewed in Refs. [4,10], the twin systems are rhombohedral (R) with Miller indices $\langle 1\bar{1}0\bar{1}\rangle\{1\bar{1}02\}$ in the structural unit cell, and basal (B) with Miller indices $\langle 1\bar{1}00\rangle\{0001\}$ in the structural unit cell. Twinning shear for R systems ($\gamma_0 = 0.202$) is less than that for B systems ($\gamma_0 = 0.635$). Surface energies for cleavage on rhombohedral, prismatic and basal planes have been reported, with R planes the most likely to cleave and B planes difficult to fracture [29]. In various phase-field simulations reported next, either a B twin system or a R twin system is active, with a mode I crack located on one of several possible planes. Specifically, the four cases reported in Table 3 correspond to (i) R twinning induced by a basal plane crack ($\boldsymbol{s}$ at $\theta = 1.07$ rad); (ii) R twinning induced by a noncrystallographic plane crack that produces maximum τ ($\boldsymbol{s}$ at $\theta = 1.22$ rad); (iii) B twinning induced by a rhombohedral plane crack ($\boldsymbol{s}$ at $\theta = 1.07$ rad); and (iv) B twinning induced by noncrystallographic plane crack that produces maximum τ ($\boldsymbol{s}$ at $\theta = 1.22$ rad). Cleavage surface energies entering $\overline{G}_C$ in Table 3 are obtained from [29]. For cases (i) and (iii), isotropic surface energy is used. For cases (ii) and (iv), the effects of anisotropic $\boldsymbol{\kappa}$ associated with incoherent twin boundary energy are explored by setting $\alpha = 100$ [21,20]. In all cases, isotropic elasticity is imposed with Voigt elastic constants, noting from previous work [10] that the effects of elastic anisotropy are small in sapphire; elastic anisotropy is also investigated later in 3-D simulations in Section 5, confirming this assertion.

Results for cases (i) and (iii) are shown in Fig. 8a and b at $\Delta > \Delta_T$. The basal twin (Fig. 8a) nucleates at a larger Δ and is thinner than the rhombohedral twin (Fig. 8b). Twinning resistance is compared with fracture energy in Table 3. Since $2\overline{\Gamma}_T \ll \overline{G}_C$ for cases (i) and (ii) involving R twinning, this twinning mode is preferred over mode I crack extension. On the other hand, $2\overline{\Gamma}_T$ is smaller than $\overline{G}_C$, but not significantly so, for cases (iii) and (iv) involving basal twinning. It follows that basal twinning is possible in such cases, but crack extension is also likely, considering possible sources of uncertainty in the phase-field model/parameters and local variations in microstructure (e.g. defects or impurities) inherent in real experimental samples. Predictions are in qualitative agreement with experiments. Specifically, in cleavage experiments [29], basal fracture was found much more difficult to induce than rhombohedral fracture. In recovered specimens fractured by bending [30] on unidentified planes, numerous thicker R twins were found, and fewer thinner B twins were observed. The thicker predicted shape of the R twin relative to the B twin is evident in Fig. 8; it has been noted elsewhere [28] that twin systems with larger γ_0 are prone to yield thinner twins. The presence of both kinds of twins has been reported in shock compression experiments on alumina polycrystals [3].

4.3. Magnesium

Magnesium is a moderately ductile metal with hexagonal crystal structure. A number of slip and twin systems

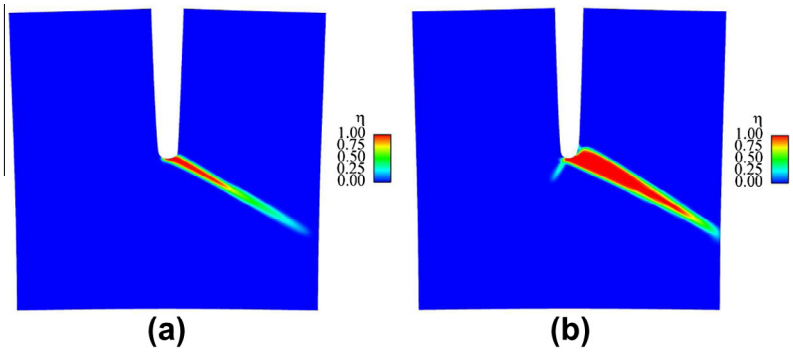

Fig. 8. Order parameter for mode I cleavage of sapphire single crystal: (a) basal twinning and rhombohedral cleavage, $\Delta = 0.057$; (b) rhombohedral twinning and basal cleavage, $\Delta = 0.046$.

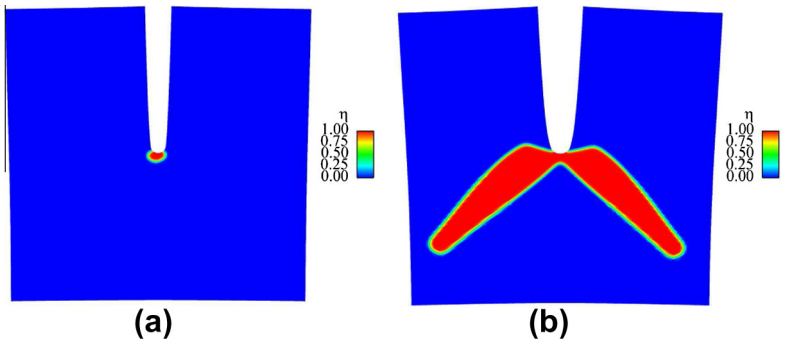

Fig. 9. Order parameter for mode I basal plane cleavage of magnesium crystal: (a) twin nucleation, $\Delta = 0.044$; (b) tensile twinning, $\Delta = 0.1$.

have been identified; the twin system investigated here is the dominant inelastic mechanism observed in single crystals stretched along [0001]: the system $\langle 10\bar{1}1\rangle\{\bar{1}012\}$, with relatively small shear $\gamma_0 = 0.1295$. Elastic anisotropy is very low in Mg; Voigt isotropic elastic constants [9] are used, along with the isotropic twin boundary surface energy listed in Ref. [9]. Although various cleavage modes in single crystals have been reported [31], quantitative values of fracture surface energies are not evident in the existing literature; however, analysis suggests that the fracture energies of prismatic and basal planes should be approximately equal [32]. In the present work, a pre-existing edge crack on the basal plane is modeled, where the value of $\overline{G}_C$ in Table 3 is obtained from the macroscopic fracture toughness of Mg polycrystals [33]. The most favorably oriented twin system is oriented with $\boldsymbol{s}$ at $\theta = 0.75$ rad.

The predicted twin is shown in Fig. 9a at $\Delta \approx \Delta_T$ and in Fig. 9b at $\Delta > \Delta_T$. The rounded shape of the twin nucleus in Fig. 9a is in qualitative agreement with previous theoretical studies [9,34]. The symmetric double-twin morphology in Fig. 9b is similar to atomic simulation results of tensile twinning in a Mg single crystal with a pre-existing center crack on the basal plane [35] (see their Fig. 4). In the present simulations, the blunt shape of the twin(s) correlates with the low value of γ_0 in Mg. Twinning resistance is compared with fracture energy in Table 3. Since $2\overline{\Gamma}_T \ll \overline{G}_C$,

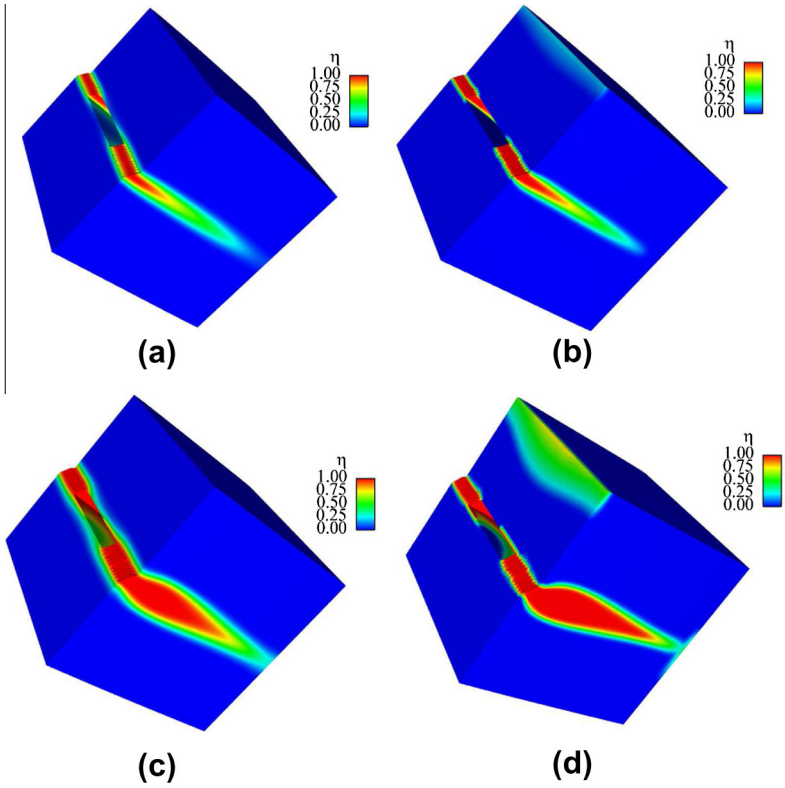

Fig. 10. Order parameter for direct shear loading ($\gamma = 1$) of sapphire single crystal with halfpenny-shaped edge notch: (a) basal twin, anisotropic elasticity and anisotropic surface energy; (b) basal twin, isotropic elasticity and isotropic surface energy; (c) rhombohedral twin, anisotropic elasticity and anisotropic surface energy; (d) rhombohedral twin, isotropic elasticity and isotropic surface energy.

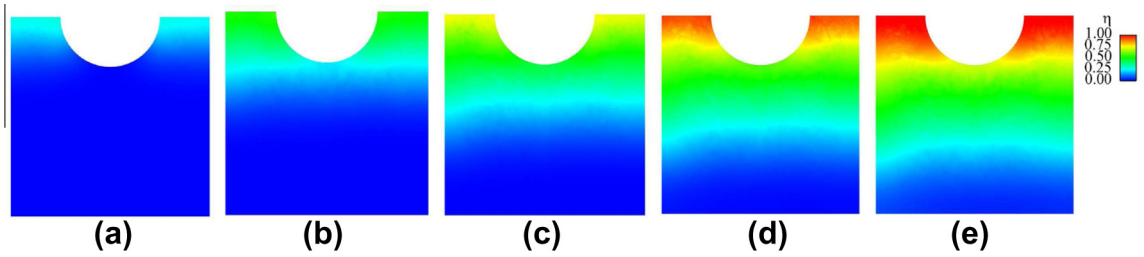

Fig. 11. Twin nucleation and growth along mid-plane $Y = 0$ for direct shear loading of sapphire single crystal, anisotropic model, basal twin: (a) $\gamma = 0.2$; (b) $\gamma = 0.4$; (c) $\gamma = 0.6$; (d) $\gamma = 0.8$; (e) $\gamma = 1.0$.

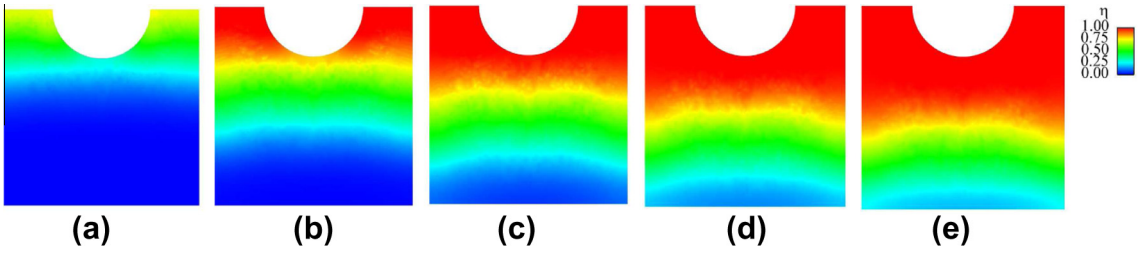

Fig. 12. Twin nucleation and growth along mid-plane $Y = 0$ for direct shear loading of sapphire single crystal, anisotropic model, rhombohedral twin: (a) $\gamma = 0.2$; (b) $\gamma = 0.4$; (c) $\gamma = 0.6$; (d) $\gamma = 0.8$; (e) $\gamma = 1.0$.

twinning is preferred over mode I crack extension for the present boundary conditions.

The analytical model of Ref. [8] suggests the following criterion for twinning vs. crack extension:

$$\chi \cdot (f_T/f_C)^{1/2} > 1 \Rightarrow \text{fracture},$$
$$\chi \cdot (f_T/f_C)^{1/2} < 1 \Rightarrow \text{twinning}, \tag{4.1}$$

where the dimensionless parameter χ depends on load direction, crystal structure (e.g. c/a ratio in hexagonal metals) and anisotropic elastic constants, and f_T and f_C are energies associated with "total inelastic resistance" against twin and crack extension, respectively. For basal plane cleavage and tensile twinning, a value of $\chi = 1.66$ is reported for Mg [8]. Values of f_T and f_C have not been reported; the former can be deduced from the present results if $f_C = \frac{1}{2} G_C$ is assumed. Squaring both sides of (4.1) and comparing with (3.15) yields

$$f_T = \Gamma_T/\chi^2 = \mu l \overline{\Gamma}_T/\chi^2 \approx 0.26 \quad \text{J/m}^2, \tag{4.2}$$

which is significantly larger than the twin boundary surface energy $\Gamma = 0.12$ J/m^2. Such a result reinforces the notion that total energetic resistance to twinning depends on other factors besides Γ alone.

5. Twinning in a notched single crystal: 3-D simulations

Three-dimensional simulations demonstrate how the phase-field model can be applied to predict twinning under complex stress states. In the present simulations of single-crystal sapphire, attention is restricted to a single potentially active twin system. Boundary conditions imposing direct, intense shear strain resolved on this system (discussed in detail below) are such that only one system would be expected to be active. Various simulations consider either rhombohedral (R) or basal (B) twinning, with isotropic or anisotropic material models. For the former, isotropic twin boundary surface energy is also used. For the latter, the trigonal elastic constants ($C_{11} = 500$, $C_{12} = 168$, $C_{13} = 121$, $C_{14} = 24$, $C_{33} = 502$, $C_{44} = 151$ GPa) from Ref. [10] are used, and anisotropic twin boundary energy is imposed with $\alpha = 100$. The remaining material properties have already been discussed in Section 4.2 in the context of Table 3.

Consider here is a cube of material with initial dimensions $4a \times 4a \times 4a$, where $a/l = 10$. Six faces are labeled $\pm X$, $\pm Y$, $\pm Z$, where the unit normal of each face is aligned parallel to the corresponding axis in a global Cartesian coordinate system with origin at the center of the cube. A half-cylinder of radius a and height $2l$ is extracted from the $-X$ face of the cube along the mid-plane $Y = 0$. This can be interpreted as a pre-existing, halfpenny-shaped notch or edge crack. Displacement boundary conditions are applied to the $-X$ face and create a region of intense shear deformation of magnitude γ over the region $-l < Y < l$, similar to conditions explored in Ref. [36] for modeling slip, or to what might be observed in the early stages of a dynamic Kalthoff experiment. Specifically, face $-X$ is held fixed for $-2a \leqslant Y \leqslant -l$ and displaced rigidly in the $+X$ direction for $l \leqslant Y \leqslant 2a$. The opposite $+X$ face is held fixed ($\boldsymbol{u} = \boldsymbol{0}$), and lateral faces $\pm Y$, $\pm Z$ are traction free. All surfaces comprising $\partial\Omega$ (six cube faces and the crack surface) are assigned the free ($h = 0$) Neumann condition for the order parameter, enabling possible twin nucleation at any of these surfaces.

Characteristic results are shown in Fig. 10 for an imposed shear of unity ($\gamma = 1$). Specifically, B twinning is depicted in Fig. 10a and b, R twinning in Fig. 10c and d. For each mode of twinning, predictions of linear isotropic and anisotropic elasticity are similar for the order parameter (η) profile in the region of intense shear. Anisotropic surface energy suppresses formation of the partial secondary twins that emerge along the upper edge of the $-X$ face in each of the isotropic simulations (Fig. 10b and d). Simulations with neo-Hookean elasticity were also performed; the results were very similar to those shown for linear isotropic elasticity and are not shown. Consistent with the results of 2-D simulations in Section 4.2 and experimental observations [30], basal twinning is more difficult to enact than rhombohedral twinning under the present direct shear boundary conditions, and B twins tend to be thinner than R twins.

Order parameter contours along mid-plane $Y = 0$ are shown in Figs. 11 and 12, respectively, for B and R twinning for incrementally increasing applied deformation γ. Some asymmetry of the twin boundary front is evident, particularly for the B twin in Fig. 11, a consequence of anisotropy. In these simulations, the semicircular edge crack does not promote or inhibit twinning; however, different boundary conditions explored elsewhere in atomic simulations of shock compression [37] have demonstrated the possibility of R twinning induced at pre-existing planar cracks in sapphire.

6. Conclusions

Twin emission from a crack tip has been studied using phase-field simulations. A parameter associated with resistance to twin nucleation under mode I/II loading has been derived. This parameter can be compared with the fracture energy of the material to suggest whether an existing crack should extend or a deformation twin should emerge and grow. Effects of material properties and phase-field model features on twinning resistance have been studied parametrically, with Poisson's ratio and elastic nonlinearity showing little effect. In contrast, resistance to crack tip twinning depends strongly on twin boundary surface energy and twinning shear. Plane-strain simulations of twinning induced by a pre-existing crack on relevant cleavage planes in calcite, sapphire and magnesium single crystals have been conducted. Results suggest that calcite should cleave, magnesium should twin, and that rhombohedral twinning is preferred to basal twinning in sapphire, all in agreement with experiment. Three-dimensional simulations of shear loading of sapphire demonstrate a preference for rhombohedral over basal twins, with the former thicker in shape, in agreement with experiment.

References

[1] Christian J, Mahajan S. Deformation twinning. Prog Mater Sci 1995;39:1–157.

[2] Tadmor E, Hai S. A Peierls criterion for the onset of deformation twinning at a crack tip. J Mech Phys Solids 2003;51:765–93.

[3] Chen M, McCauley J, Dandekar D, Bourne N. Dynamic plasticity and failure of high-purity alumina under shock loading. Nature Mater 2006;5:614–8.

[4] Clayton J. A continuum description of nonlinear elasticity, slip and twinning, with application to sapphire. Proc Roy Soc Lond A 2009;465:307–34.

[5] Garber R, Stepina E. Rules governing the motion of dislocations during deformation twinning. Soviet Phys Solid State 1965;5:152–8.

[6] Wong T, Bradt R. Microhardness anisotropy of single crystals of calcite, dolomite, and magnesite on their cleavage planes. Mater Chem Phys 1992;30:261–6.

[7] Rice J. Dislocation nucleation from a crack tip: an analysis based on the Peierls concept. J Mech Phys Solids 1992;40:239–71.

[8] Yoo M. Slip, twinning, and fracture in hexagonal close-packed metals. Metall Trans A 1981;12:409–18.

[9] Clayton J, Knap J. A phase field model of deformation twinning: nonlinear theory and numerical simulations. Physica D 2011;240:841–58.

[10] Clayton J, Knap J. Phase field modeling of twinning in indentation of transparent single crystals. Mod Sim Mater Sci Eng 2011;19:085005.

[11] Clayton J. Nonlinear mechanics of crystals. Dordrecht: Springer; 2011.

[12] Boulbitch A, Tolédano P. Phase nucleation of elastic defects in crystals undergoing a phase transition. Phys Rev Lett 1998;81:838–41.

[13] Boulbitch A, Korzhenevskii A. Self-oscillating regime of crack propagation induced by a local phase transition at its tip. Phys Rev Lett 2011;107:085505.

[14] Idesman A, Levitas V, Stein E. Structural changes in elastoplastic material: a unified finite-element approach to phase transformation, twinning and fracture. Int J Plast 2000;16:893–949.

[15] Aranson I, Kalatsky V, Vinokur V. Continuum field description of crack propagation. Phys Rev Lett 2000;85:118–21.

[16] Jin Y, Wang Y, Khachaturyan A. Three-dimensional phase field microelasticity theory and modeling of multiple cracks and voids. Appl Phys Lett 2001;79:3071–3.

[17] Karma A, Kessler D, Levine H. Phase-field model of mode III dynamic fracture. Phys Rev Lett 2001;87:045501.

[18] Spatschek R, Hartmann M, Brener E, Müller-Krumbhaar H. Phase field modeling of fast crack propagation. Phys Rev Lett 2006;96:015502.

[19] Spatschek R, Brener E, Karma A. Phase field modeling of crack propagation. Philos Mag 2011;91:75–95.

[20] Hildebrand F, Miehe C. A phase field model for the formation and evolution of martensitic laminate microstructure at finite strains. Philos Mag 2012;92:4250–90.

[21] Hu S, Henager C, Chen L-Q. Simulations of stress-induced twinning and de-twinning: a phase field model. Acta Mater 2010;58:6554–64.

[22] Levitas V, Levin V, Zingerman K, Freiman E. Displacive phase transitions at large strains: phase-field theory and simulations. Phys Rev Lett 2009;103:025702.

[23] Rice J. Mathematical analysis in the mechanics of fracture. In: Liebowitz H, editor. Fracture: an advanced treatise. New York: Academic Press; 1968. p. 191–311.

[24] Bilby B, Bullough R. The formation of twins by a moving crack. Philos Mag 1954;45:631–46.

[25] Bueble S, Schmahl W. Mechanical twinning in calcite considered with the concept of ferroelasicity. Phys Chem Minerals 1999;26:668–72.

[26] Gilman J. Direct measurements of the surface energy of crystals. J Appl Phys 1960;31:2208–18.

[27] Santhanam A, Gupta Y. Cleavage surface energy of calcite. Int J Rock Mech Mining Sci Geo Abstr 1968;5:253–9.

[28] Cahn R. Plastic deformation of alpha-uranium; twinning and slip. Acta Metall 1953;1:49–70.

[29] Wiederhorn S. Fracture of sapphire. J Am Ceram Soc 1969;52:485–91.

[30] Heuer A. Deformation twinning in corundum. Philos Mag 1966;13:379–93.
[31] Reed-Hill R, Robertson W. The crystallographic characteristics of fracture in magnesium single crystals. Acta Metall 1957;5:728–37.
[32] Yoo M. The elastic energy of slit cracks in hexagonal crystals. Scr Metall 1979;13:131–6.
[33] Somekawa H, Inoue T, Mukai T. Deformation mechanism near crack-tip by finite element analysis and microstructure observation in magnesium alloys. Mater Sci Eng A 2010;527:1761–8.
[34] Wang J, Hoagland R, Hirth J, Capolungo L, Beyerlein I, Tomé C. Nucleation of a (1012) twin in hexagonal close-packed crystals. Scripta Mater 2009;61:903–6.
[35] Tang T, Kim S, Horstemeyer M, Wang P. Atomistic modeling of crack growth in magnesium single crystal. Eng Fract Mech 2011;78:191–201.
[36] Gumbsch P, Gao H. Dislocations faster than the speed of sound. Science 1999;283:965–8.
[37] Kuksin A, Yanilkin A. Formation of twins in sapphire under shock wave loading: atomistic simulations. J Appl Phys 2012;111:033513.

NO. OF COPIES	ORGANIZATION
1 (PDF)	DEFENSE TECHNICAL INFORMATION CTR DTIC OCA
1 (PDF)	DIRECTOR US ARMY RESEARCH LAB IMAL HRA
1 (PDF)	DIRECTOR US ARMY RESEARCH LAB RDRL CIO LL
1 (PDF)	GOVT PRINTG OFC A MALHOTRA

ABERDEEN PROVING GROUND

NO. OF COPIES	ORGANIZATION
35 (PDF)	DIR USARL
	RDRL CIH C
	P CHUNG
	J KNAP
	RDRL WM
	B FORCH
	J MCCAULEY
	P PLOSTINS
	RDRL WML B
	I BATYREV
	B RICE
	D TAYLOR
	N WEINGARTEN
	RDRL WML H
	B SCHUSTER
	RDRL WMM
	J BEATTY
	RDRL WMM B
	G GAZONAS
	C RANDOW
	T SANO
	RDRL WMM E
	J SWAB
	RDRL WMM F
	M TSCHOPP
	RDRL WMP
	S SCHOENFELD
	RDRL WMP B
	C HOPPEL
	D POWELL
	S SATAPATHY
	M SCHEIDLER
	T WEERISOORIYA
	RDRL WMP C
	R BECKER
	S BILYK
	T BJERKE
	D CASEM
	J CLAYTON
	D DANDEKAR
	M GREENFIELD
	R LEAVY
	M RAFTENBERG
	S SEGLETES
	C WILLIAMS
	RDRL WMP D
	R DONEY
	RDRL WMP E
	S BARTUS